Widespread stratospheric intrusion influence on summer ozone pollution over China revealed by multi-site ozonesondes~~, ground-based measurement~~ and ~~fully-~~validated EAC4 reanalysis

Zhiheng Liao[1], Jinqiang Zhang[2], Meng Gao[3], Zhiqiang Ma[1]

1 Institute of Urban Meteorology, China Meteorological Administration, Beijing, China

2 State Key Laboratory of Atmospheric Environment and Extreme Meteorology~~Key Laboratory of Middle Atmosphere and Global Environment Observation~~, Institute of Atmospheric Physics, Chinese Academy of Sciences, Beijing, China

3 Department of Geography, Hong Kong Baptist University, Hong Kong SAR, China

Correspondence: Z. Ma (zqma@ium.cn)

Abstract

Understanding stratospheric intrusion (SI) is crucial for elucidating atmospheric complexities and improving strategies to mitigate surface ozone (O_3) pollution. This study investigates a deep trough-induced SI event in China from June 10 to 13, 2013, based on ozonesondes from Beijing, Changchun, and Hong Kong, ~~nationwide ground-based measurements,~~ and ~~fully-~~validated O_3 reanalysis products. Ozonesondes from Beijing indicated notable ~~high-level~~upper-level secondary O_3~~ozone~~ peaks (> 400 ppbv) since June 11. Tropospheric sub-high ~~ozone~~ O_3 layers were observed in Changchun on June 12 (> 120 ppbv) and Hong Kong on June 13 (> 80 ppbv). Nationwide surface ~~ozone~~ measurements recorded severe ~~ozone~~ O_3 pollution (> 100 ppbv) from western plateaus to eastern plains over China. Together, these observations suggest a widespread influence of stratospheric ~~ozone~~ O_3 intrusion. Further, the ozonesonde-validated EAC4 reanalysis reproduced the fine-scale SI structure (O_3-rich "tongue"), in turn well explaining the secondary ~~ozone~~ O_3 peaks and sub-high ~~ozone~~ O_3 layers in ozonesonde observations. The O_3-rich "tongue" swept through the Tibetan Plateau on June 10, triggering extreme ~~ozone~~ O_3 pollution with a stratospheric ~~ozone~~ contribution up to 30 ppbv (>30 %). With the trough's eastward movement, the O_3-rich "tongue" penetrated into the lower troposphere of eastern China, and then ~~be~~ entrained into the surface layer, exacerbating ~~severe~~ surface ~~ozone~~ O_3 pollution occurred in eastern China~~the Northern China Plain~~ on June 13, with a stratospheric ~~ozone~~ O_3 contribution of 3–15 ppbv (2–10 %). This research underscores the importance of multi-site ozonesondes in understanding stratospheric ~~ozone~~ O_3 intrusions and the potential of the publicly available EAC4 reanalysis in multiyear SI analyses.

Keywords: stratospheric intrusion; secondary ozone peak; surface ozone pollution; ~~high-level~~upper-level trough; contribution

1 Introduction

Surface ozone (O_3) poses significant risks to public health and ecosystem productivity due to its strong oxidative ~~properties~~ capacity (Monks et al., 2015). While O_3 in the lower atmosphere is predominantly produced through photochemical reactions, stratospheric intrusion (SI)—the process where O_3-rich air masses from the stratosphere descend to the lower troposphere—can also increase surface O_3 concentrations in certain regions (Akritidis et al., 2018;Skerlak et al., 2019;Dreessen, 2019). The natural SI processes complicate efforts to manage and reduce anthropogenic O_3 pollution (Zhao et al., 2025). Therefore, quantifying the SI contribution to surface O_3 is essential for developing effective air quality management strategies~~understanding how SI affects surface O_3 is crucial for improving strategies to mitigate O_3 pollution~~.

SI is a key component of extratropical weather processes, and detecting SI events along with their influence on tropospheric chemistry has been a major scientific ~~concern~~ focus ~~since the 1970s~~across Europe (Appenzeller and Davies, 1992;Stohl et al., 2003;Akritidis et al., 2018), North America (Hocking et al., 2007;Lin et al., 2016;Wang et al., 2020b), East Asia (Lin et al., 2021;Liu et al., 2024;Chen et al., 2024), and other extratropical regions (Zhang et al., 2024). ~~(Zhang et al., 2024;Lin et al., 2021;Ma et al., 2014;Appenzeller and Davies, 1992;Stohl et al., 2003;Hocking et al., 2007;Lin et al., 2016;Liu et al., 2024).~~ (Appenzeller and Davies (1992);Hocking et al. (2007);Lin et al. (2016))While observational evidence confirms that SI can trigger episodic spikes in surface O_3 concentrations~~Numerous evidences have shown that surface O_3 concentrations can episodically rise during the SI event (Cristofanelli et al., 2010;Langford et al., 2012;Yates et al., 2013;Lin et al., 2015;Dreessen, 2019;Ou-Yang et al., 2022;Chen et al., 2023;Chen et al., 2024).~~ (Cristofanelli et al., 2010;Langford et al., 2012;Yates et al., 2013;Lin et al., 2015;Dreessen, 2019;Ou-Yang et al., 2022;Chen et al., 2023;Chen et al., 2024), accurately quantifying this phenomenon remains difficult due to observational limitations. Traditionally, ozonesondes have served as a primary tool for SI detection, as they provide complete vertical O_3 profiles up to approximately 35 km. However, their sparse temporal and spatial coverage hinders a comprehensive understanding of how stratospheric O_3 penetrates to the surface~~the detailed structure of stratospheric ozone intrusion into the surface layer remains poorly understood due to limited ozonesonde measurements~~ (Chen et al., 2011;Zhao et al., 2021;Hong et al., 2024)~~. Consequently,~~. ~~the stratospheric intrusion contribution to surface ozone has long been a topic of much debate over the past few decades (Stohl et al., 2003;Yang et al., 2022;Zheng et al., 2024). Up to now~~To date, much of the current understanding of SI and its role in surface O_3 pollution~~understanding of SI and its contribution to surface O_3 pollution comes~~ has been derived from satellite observations (Li et al., 2015;Zhang et al., 2022;Jaeglé et al., 2017), atmospheric reanalysis (Chen et al., 2023;Knowland et al., 2017;Bartusek et al., 2023;Akritidis et al., 2018), and model simulations (Wang et al., 2020a;Zhao et al., 2021;Zhang et al., 2022;Chang et al., 2023;Hong et al., 2024;Luo et al., 2024;Zhao et al., 2024;Zhu et al., 2024;Skerlak et al., 2019). Yet, these approaches often lack rigorous validation against ozonesonde data, leading to substantial uncertainties in their findings~~Although open-source products and custom model simulations show a certain ability in capturing the stratospheric ozone intrusion and even quantifying the stratospheric intrusion contribution, their results still possess large uncertainties due to a common dearth of validation against with vertical O_3 measurements~~. ~~Besides~~Alternatively,~~,~~ ~~recent~~ some studies have attempted to quantify stratospheric influences using ground-based chemical tracers~~attempts to quantify stratospheric influences using ground-based chemical tracers~~, e.g., the ratio of O_3 to CO (O_3/CO) (Ma et al., 2014;Chen et al., 2024), cosmogenic sulfur-35 (^{35}S) (Lin et al., 2016;Lin et al., 2021), and the ratio of cosmogenic beryllium-10 to beryllium-7 ($^{10}Be/^{7}Be$) (Jordan et al., 2003;Liu et al., 2024). However, these methods also exhibit limitations, as ground-based measurements alone cannot fully resolve the vertical structure of SI aloft~~also have embedded uncertainties because little is known about the SI structure aloft from the ground-based measurements alone~~ (Zheng et al., 2024). Moreover, inconsistencies arise when different tracers are applied—for instance, while one study using ^{35}S~~Opposite conclusions were even drawn from different chemical tracers. For example,~~ ~~an isotopic (^{35}S) chemical tracer study~~ (Lin et al., 2021) suggested a west-high-east-low SI contribution pattern over China~~revealed a west-high-east-low stratospheric intrusion contribution over China~~, another study based on the~~whereas an~~ O_3~~O_3~~/CO ~~chemical tracer study~~ratio (Chen et al., 2024) reported the opposite distribution~~suggested an inverse distribution~~. These conflicting results reveal a significant research gap, emphasizing the necessity for comprehensive analysis of multi-platform datasets to advance our understanding of stratospheric O_3 intrusion and its effects on surface O_3 pollution.~~The lack of consensus lead to a significant cognitive confusion, emphasizing the urgent need of direct ozonesonde observations to refine the fundamental understanding of stratospheric ozone intrusion and its contribution to surface ozone pollution.~~

This study examines a representative SI event triggered by an upper-level trough over China during 10-13 June 2013. The event was characterized by severe surface O_3 pollution that sequentially occurred in the high-altitude Tibetan Plateau and low-lying eastern China.~~This study focuses on a typical SI event associated with an upper-level trough observed over China during June 10–13, 2013, to investigate its influence on summer ozone pollution. During this event, nationwide air quality measurements performed by the China National Environmental Monitoring Centre recorded severe surface ozone pollution (exceeding 100 ppbv) from the high-elevation Tibetan Plateau to the low-altitude eastern China.~~ To investigate the potential connection between SI processes and these O_3 pollution episodes, ~~We~~ we employed a multi-platform integrated approach combining multi-site ozonesondes~~conducted intensive ozonesonde observations (daily resolution) in Beijing and Changchun, and collected routine ozonesonde (weekly resolution) in Hong Kong.~~, ground-based O_3 measurements, satellite O_3 products, and atmospheric O_3 reanalysis. Through comprehensive analysis of this multi-platform datasets, we aim to address two key scientific objectives:~~Through detailed analysis of multi-site ozonesondes, ground-based measurements, and fully-validated reanalysis products (*Datasets*) in this SI event, this study aims to~~ 1) to characterize the spatiotemporal evolution of trough-induced stratospheric O_3 intrusion~~spatial and temporal behavior of upper-level trough-induced stratospheric ozone intrusion~~, 2) to quantitatively assess the SI contribution to surface O_3 pollution over different regions~~quantify its contribution to surface ozone pollution, and 3) elucidate the underlying dynamical transport mechanisms~~.

2 Datasets

2.1 Ozonesonde observation

~~Ozonesondes provide a detailed vertical ozone profiles and thus are an important tool for quantifying the vertical distribution of ozone and therefore have been useful in validating satellite retrievals of ozone and atmospheric ozone reanalysis products.~~ In China, ozonesondes, along with radiosondes, were routinely launched weekly in Beijing (116.47 °E, 39.80 °N~~; 33 m above mean sea level (MSL)~~) and Hong Kong (114.17 °E, 22.31 °N~~; 66 m above MSL~~). During June 2013, an intensive ozonesonde ~~launch~~ experiment was held in Beijing and Changchun (125.20 ° E, 43.90 ° N~~; 237 m above MSL~~), with consecutive launches from June 10–13. The details of the ozonesonde experiment can be found in Zhang et al. (2013). These sondes (including the routine ozonesonde in Hong Kong) were launched around 13:30 China Standard Time~~ (CST)~~, providing high-resolution profiles of ~~ozone~~ O_3 partial pressure, atmospheric pressure, temperature, and humidity from the surface up to approximately 35 km (Zhang et al., 2021;Liao et al., 2024). For this study, data from nine ozonesonde observations were analyzed to examine stratospheric ~~ozone~~ O_3 intrusion during June 10–13, 2013, including four consecutive days in Beijing and Changchun, and a single launch on June 13 in Hong Kong. By comparing the sonde-based surface O_3 concentrations with ground-based O_3 measurements (Fig. 3B), we demonstrated a good accuracy of these ozonesonde observations (R = 0.981, and MAB = 3.2 ppbv).

2.2 Atmospheric reanalysis data

ERA5, the fifth-generation ECMWF (European Centre for Medium-Range Weather Forecasts) global reanalysis, offers a comprehensive dataset at a spatial resolution of 0.25 ° × 0.25 ° and a temporal resolution of 1 hour for climate and weather analysis (Hersbach et al., 2020). It integrates model data with observations using four-dimensional variational assimilation~~ (4D-Var)~~ in ECMWF's Integrated Forecast System (IFS). This study utilized ERA5 data, including geopotential height, potential vorticity, ~~vertical velocity,~~ and wind fields, to describe the synoptic conditions during the stratospheric intrusion event.

EAC4 (ECMWF Atmospheric Composition Reanalysis 4) represents the fourth generation of ECMWF's

atmospheric composition reanalysis, with a spatial resolution of 0.75°×0.75° and a temporal resolution of 3 hours (Inness et al., 2019). EAC4 assimilates data from various satellite sources, including total column ~~ozone~~ O_3 from the Ozone Monitoring Instrument ~~(OMI)~~ and Global Ozone Monitoring Experiment-2 ~~(GOME-2)~~ on Metop satellites, profile data from the Microwave Limb Sounder ~~(MLS)~~, and partial columns from Solar Backscatter Ultra-Violet ~~(SBUV/2)~~ and Ozone Mapping and Profiler Suite ~~(OMPS)~~. Note that surface O_3 measurements and ozonesonde O_3 profile data in China are not assimilated into the EAC4 reanalysis. The IFS used in EAC4 incorporates an extended version of the Carbon Bond 2005 ~~(CB05)~~ chemical mechanism, which includes 126 tropospheric reactions. The emission datasets are composed of anthropogenic emissions from the MACCity inventory (Granier et al., 2011), biogenic emissions from MEGAN2.1 model (Guenther et al., 2006), and biomass burning emissions from the Global Fire Assimilation System (Kaiser et al., 2012). ~~EAC4 provides both~~Apart from ~~ozone (~~O_3~~)~~, the~~and~~ stratospheric ~~ozone~~ O_3 tracer (O_3S, O_3 originating from the stratosphere) is also provided in EAC4 reanalysis. This study employed both O_3 and O_3S to characterize the three-dimensional structure of stratospheric ~~ozone~~ O_3 intrusion.

2.3 Auxiliary data

Additional data sources included ground-based ~~ozone~~ O_3 measurements from the China National Air Quality Monitoring Network and the Hong Kong Environmental Protection Department, satellite cloud images from the Moderate Resolution Imaging Spectroradiometer (MODIS), ~~Level-3~~satellite O_3~~ozone~~ ~~profile~~ products from the Atmospheric Infrared Sounder (AIRS) (Aumann et al., 2003), and atmospheric O_3~~ozone~~ reanalysis ~~products~~ from the Modern-Era Retrospective Analysis for Research and Applications, Version 2 (MERRA2) (Gelaro et al., 2017). According to previous studies (Jaeglé et al., 2017;Knowland et al., 2017;Zhang et al., 2022), we used satellite O_3 retrieved from AIRS Level 3 product, which has a spatial resolution of $1^{o}\times1^{o}$. In contrast, the MERRA2 reanalysis has a spatial resolution of 0.5°×0.625°. Both AIRS and MERRA2 O_3 products served as alternative references to EAC4 O_3 reanalysis to provide a large-scale view of horizontal and vertical O_3 structures during the SI event. Hourly surface ~~o~~ O_3~~zone~~ concentrations from ~~76~~ 77 cities~~–~~ in China (including Hong Kong) ~~during June 10–13, 2013,~~ were used to assess nationwide O_3~~ozone~~ pollution during the stratospheric intrusion event. ~~MODIS satellite cloud images illustrated the weather conditions, while AIRS and MERRA2 ozone products served as alternative references to EAC4 data.~~

3 Results

3.1 Ozonesonde evidence of stratospheric O_3~~ozone~~ intrusion

Fig. 1 illustrates the evolution of the ~~high-level~~upper-level trough event from June 10 to 13, 2013. On June 10, the upper-level trough extended from the Mongolian Plateau towards the Tibetan Plateau. By June 11, the trough had moved eastward and deepened into a "V-shaped" structure between 90°E and 120°E, causing an extremely distorted westerly jet and strong northerlies at the western flank of the trough. On this day, the emerged 1.5 PVU potential vorticity contours at 400 hPa provide convincing evidence for a deep stratospheric intrusion. On June 12, the "V-shaped" trough persisted at 200 hPa. By June 13, the ~~high-level~~upper-level trough had weakened to be a shallow structure over the North China Plain (NCP). Three-dimensional dynamics associated with upper-level troughs involves stratospheric dry intrusion (SDI) and warm conveyor belts (WCB) airstreams (Browning and Roberts, 1994;Browning, 1997). The SDI originates in the lower stratosphere on the cold side of the trough (west of the trough axis) and descends behind the cold front, while the WCB originates in the warm sector of the trough (east of the trough axis), ascending rapidly to the mid- and upper troposphere. During this event, these contrasting airstreams led to significantly different weather conditions at the two sides of the trough, with cloudy weather in the WCB zone (east) and clear weather in the SDI zone (west). There appeared an obvious transition from cloudy to

clear weather in the eastern China with the eastward movement of upper-level trough. On June 13, China, excluding the northeast and eastern coastal regions, experienced clear weather.

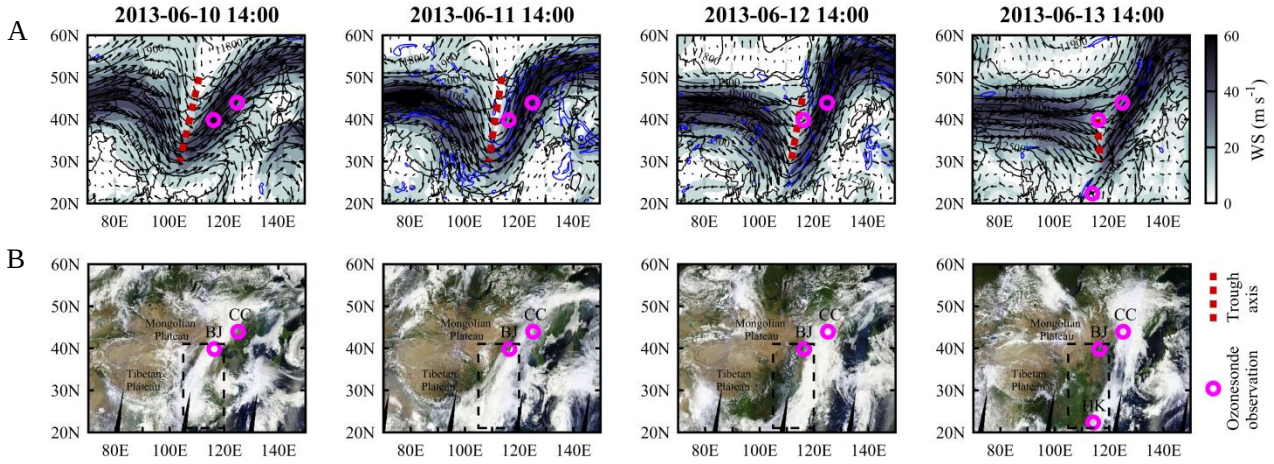

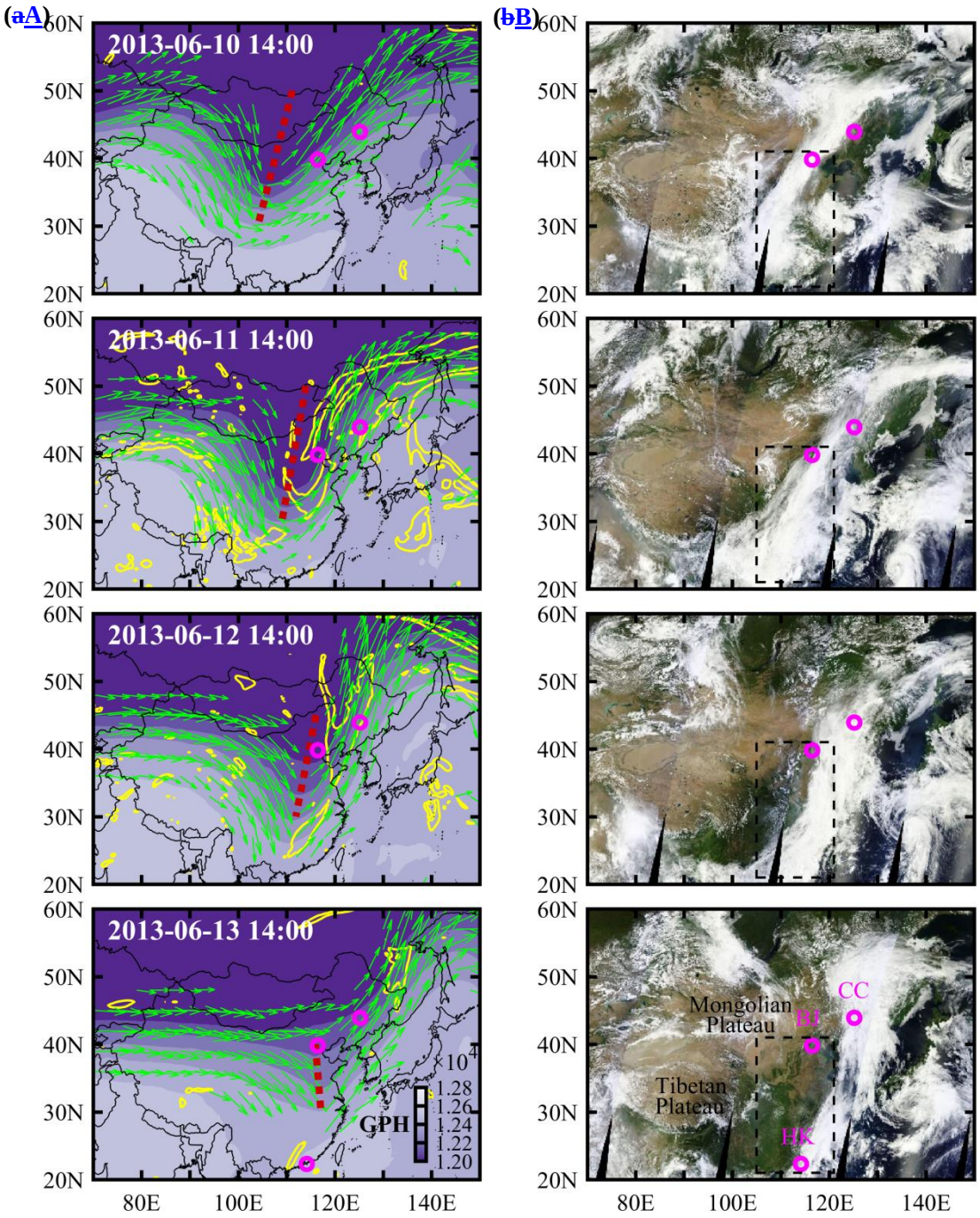

Fig. 1. (aA) Horizontal distribution of geopotential height (black contoursshading, units in gpm), wind speed (shading, units in m s^{-1}), and wind direction of jet stream in excess of 20 m s^{-1} (arrows) at 200 hPa, and potential vorticity of 1.5 PVU (blue contours, 1.5 PVU) at 400 hPa. (bB) MODIS satellite cloud images with the dashed box marking eastern China (105 °E–120121 °E, 21 °N–41 °N). Red dot lines in (A) denote the axis of upper-level trough at 200 hPa. Magenta circles mark the available ozonesondes at different sites (BJ: Beijing, CC: Changchun, and HK: Hong Kong) on different days.

Stratospheric ozone intrusion remains uncertain due to sharp spatial gradients and high variability in ozone concentrations caused by competing transport and mixing processes near the extratropical tropopause (Skerlak et al., 2019). Previous ozonesonde-based observational studies (Lemoine, 2004;Hwang et al., 2007;Chen et al., 2011;Ojha

et al., 2017) revealed that secondary O_3 peak in a height range between 9 and 16 km (i.e., near the tropopause) is a characteristic O_3-profile structure when SI occurs and triggers tropopause folding. The continuous and multi-site ozonesondes in this study provided a unique opportunity to characterize stratospheric O_3~~ozone~~ intrusion linked to upper-level trough from an observational perspective (Fig. 2). On June 10, before the trough arrived, Beijing was influenced by WCB airstreams, showing high relative humidity (~~RH~~ > 60%) in the upper troposphere. By June 11, Beijing was near the trough axis, and the O_3-rich SDI airstream began to affect the upper atmosphere, creating a secondary O_3~~ozone~~ peak (~400 ppbv at 9.5 km height) just above the rapidly descended thermal tropopause (which dropped from 10.5 km on June 10 to 8.2 km on June 11). ~~Hwang et al. (2007)~~Besides, ~~stratospheric intrusion led to~~the cold dry air of the SDI lead to a quick drop in ~~relative humidity~~relative humidity from 70% on June 10 to below 25 % on June 11 in the upper troposphere of Beijing. On June 12 and 13, the secondary O_3~~ozone~~ peaks continued to be observed over Beijing, with peak concentrations rising to 650 ppbv by June 13, but the altitude of these peaks gradually increased up to 13.6 km by June 13 with the ~~elevation~~ increase of thermal tropopause height. ~~High-level secondary ozone peaks are a characteristic O_3-profile structure associated with tropospheric folding, a major form of SI in the extratropical region (Lemoine, 2004;Hwang et al., 2007;2011;Chen et al., 2011;Ojha et al., 2017;Bartusek et al., 2023).~~ Unlike that in Beijing, the sonde-based O_3 profiles in Changchun showed ~~high-level~~ secondary O_3~~ozone~~ peak only in June 13, when ~~high-level~~upper-level trough moved eastward to affect Changchun. However, sub-high O_3~~ozone~~ layer (> 120 ppbv) appeared in the middle troposphere (4.2–8.1 km height, the shaded light gray in Fig. 2) in advance on June 12, accompanied by extremely low relative humidity. This sub-high O_3 layer is likely the transport result of pre-intruded O_3 from stratosphere over Beijing or its surroundings. Similar sub-high O_3~~ozone~~ layer (> 80 ppbv) also occurred in the lower troposphere (3.5–6.0 km height, the shaded light gray in Fig. 2) of Hong Kong (a subtropical city) on June 13. These high-O_3~~ozone~~ and low-humidity air masses in the troposphere reflect obvious stratospheric origin, suggesting a widespread SI influence from extratropics to subtropics during this deep trough ~~process~~event.

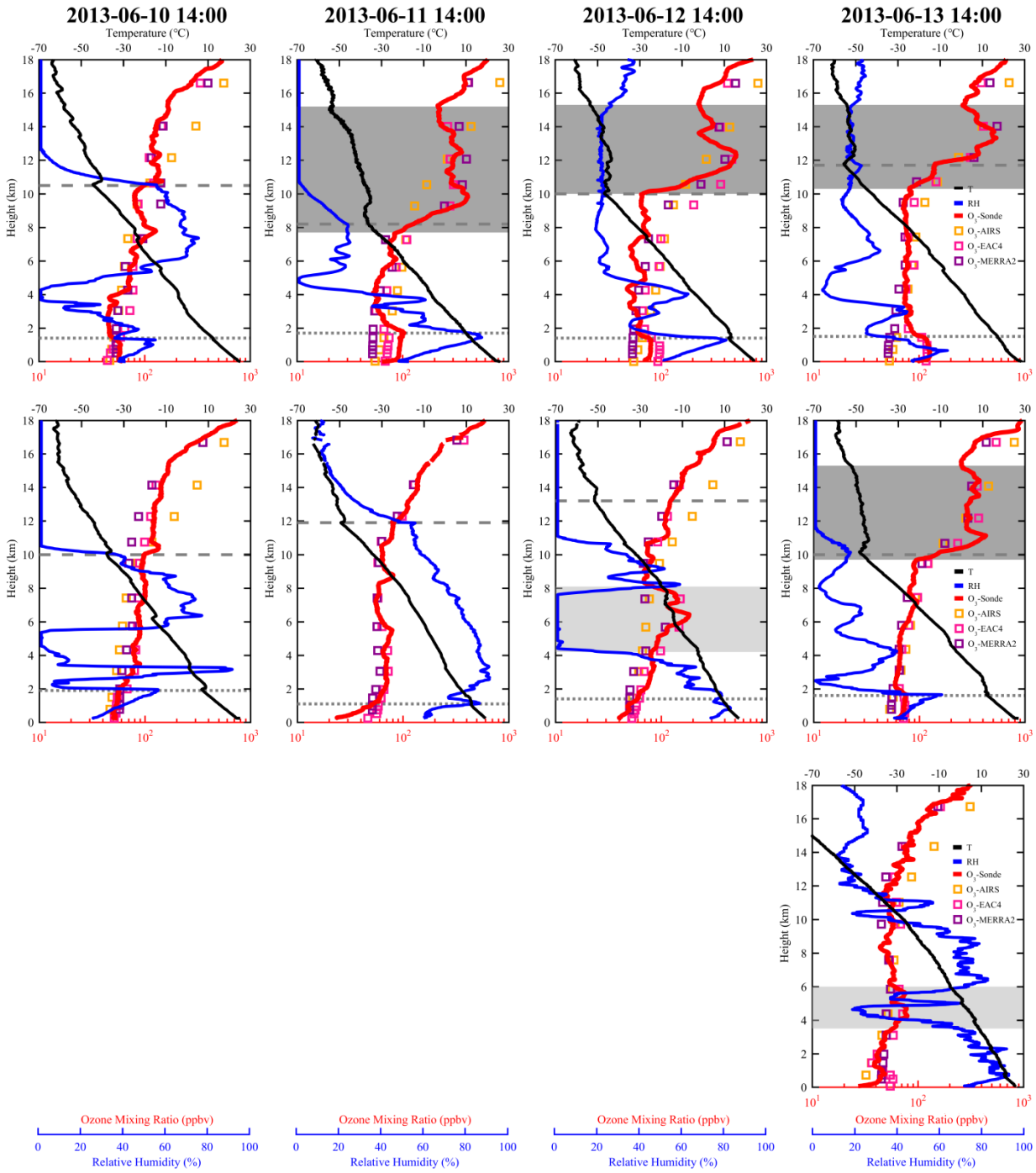
2013-06-10 14:00
2013-06-11 14:00
2013-06-12 14:00
2013-06-13 14:00
Temperature (°C)
Height (km)
T
RH
O3-Sonde
O3-AIRS
O3-EAC4
O3-MERRA2
Ozone Mixing Ratio (ppbv)
Relative Humidity (%)

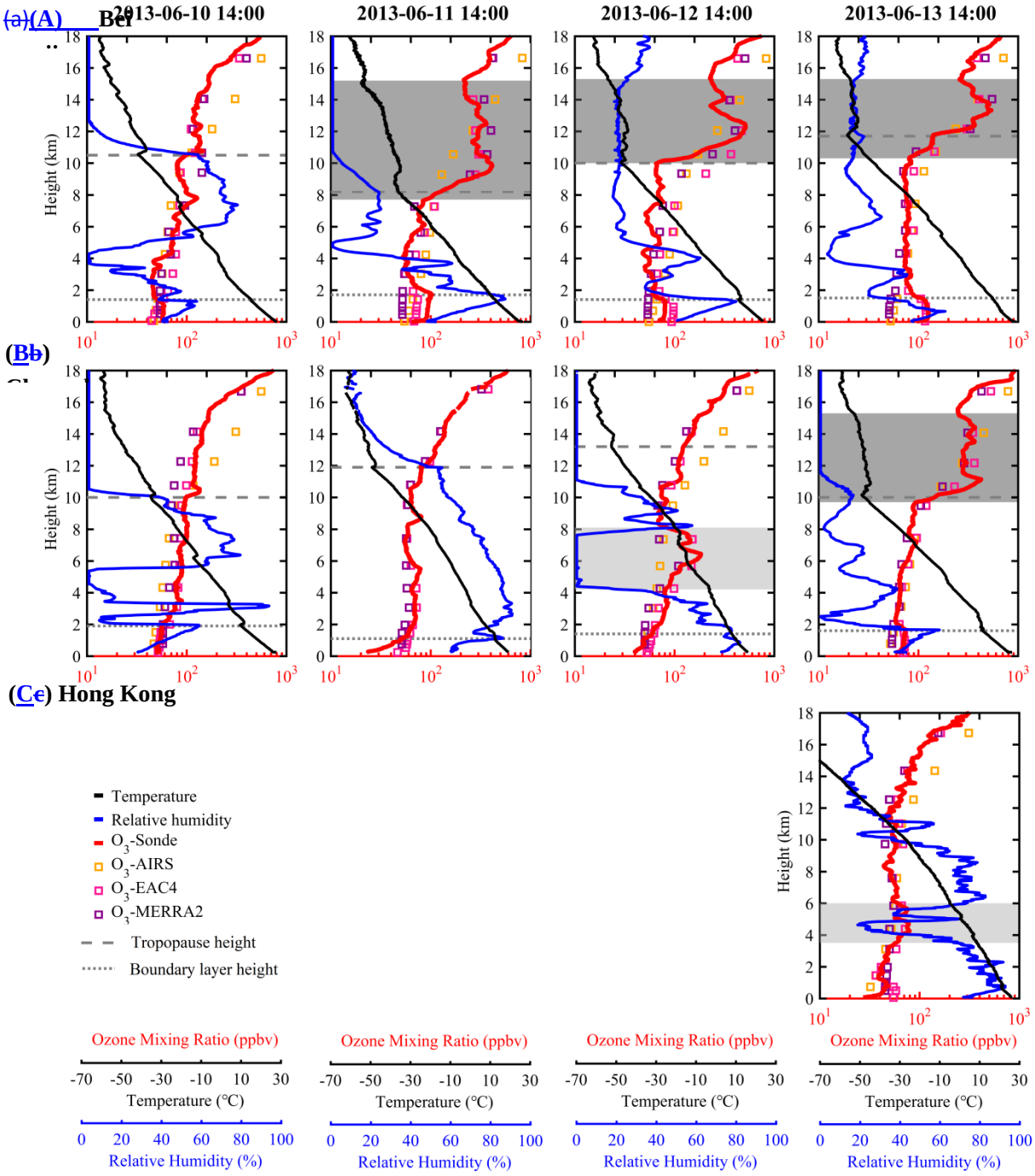

Fig. 2. O_3~~Ozone~~ vertical distribution over (A) Beijing, (B) Changchun, and (C) Hong Kong derived from ozonesonde and other data sources (including AIRS satellite observation, EAC4 and MERRA2 reanalysis) during 10–13 June 2013. Black and blue lines denote the sonde-based temperature (T) and relative humidity (RH) profiles, respectively. Gray dashed lines represent the thermal tropopause height, and gray dot lines indicate the boundary layer top height. ~~High-level~~Upper-level secondary O_3~~ozone~~ peaks are shaded heavy gray, and SI-induced O_3-rich layer in the troposphere is shaded light gray.

3.2 Three-dimensional structure of stratospheric O_3~~ozone~~ intrusion

The multi-site ozonesonde observations only provide a snapshot of stratospheric O_3~~ozone~~ intrusion~~ at its influence scale~~. To further visualize ~~the~~ its three-dimensional structure~~ of the stratospheric ozone intrusion~~, we introduced the

commonly-used ~~large-scale~~ O_3~~ozone~~ products, including AIRS satellite observation, MERRA2 and EAC4 reanalysis (Li et al., 2015;Knowland et al., 2017;Akritidis et al., 2018). ~~Before utilizing these large-scale ozone products, w~~T~~e validated~~ hese three large-scale O_3 products~~them~~ were firstly validated against our ozonesonde observations. As shown in Fig. 2, AIRS satellite observation missed the upper-level secondary O_3~~ozone~~ peaks and the boundary-layer O_3~~ozone~~ enhancements. MERRA2 reanalysis captured the secondary O_3~~ozone~~ peaks but still showed large negative biases to the observed boundary-layer O_3~~ozone~~ enhancements. In contrast, EAC4 reanalysis reproduced well the major features of the O_3~~ozone~~ vertical distribution, including upper~~upper~~-level secondary O_3~~ozone~~ peaks and boundary-layer O_3~~ozone~~ enhancements. Particularly, EAC4 exactly captured the SI-induced sub-high O_3~~ozone~~ layers~~s~~ in the middle troposphere of Changchun (on June 12) and the lower troposphere of Hong Kong (on June 13). This qualitative comparison suggests that EAC4 had a powerful ability to reproduce both the SI dynamics and boundary-layer photochemical processes. The scatter comparison with quantitative statistics~~– (~~in ~~Table~~ Fig. 3A~~1)~~ further ~~reveal~~ demonstrate that EAC4 O_3~~ozone~~ reanalysis had the strongest correlation (R = 0.947), the lowest mean absolute bias (MAB = 19.1 ppbv), the lowest root mean square error (RMSE = 36.9 ppbv), and the largest index of agreement (IOA = 0.985) to the ozonesonde observation. ~~The MAB was even comparable to that in specific model studies (Hu et al., 2017;Wang et al., 2022). Overall, T~~this sonde-based validation (Fig. 3A), along with ~~subsequent~~ validation against with nationwide ~~surface~~ ground-based O_3~~ozone~~ observations (Fig. ~~4A~~3B and Fig. 5A ~~and Table 1~~), provides us enough confidence in adopting EAC4 reanalysis to explore the three-dimensional structure of trough-induced stratospheric O_3~~ozone~~ intrusion ~~on a larger spatial scale~~.

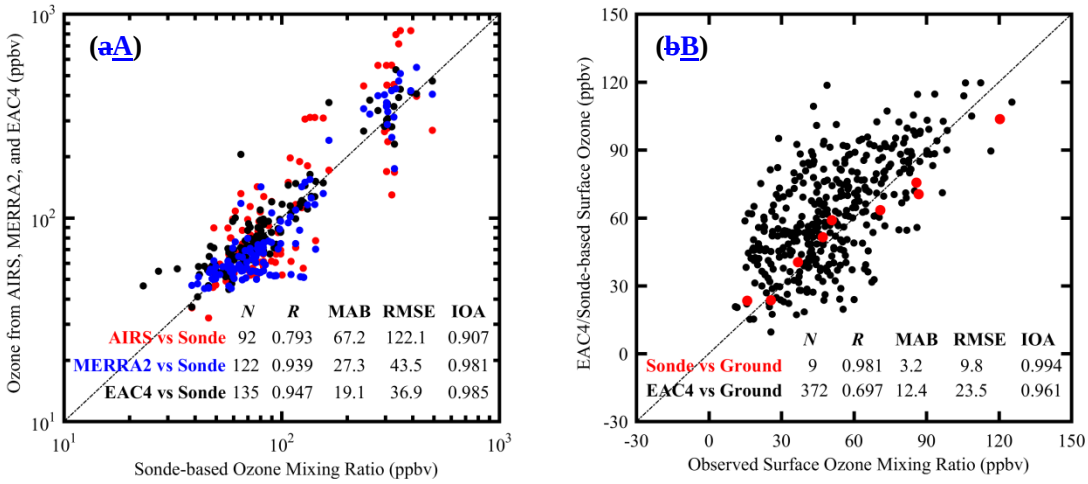

Fig. 3. (~~a~~A) Validation of AIRS, MERRA2, and EAC4 O_3 products with 9 ozonesonde observations from Beijing, Changchun, and Hong Kong. (~~b~~B) Validation of EAC4/Sonde-based surface O_3 concentrations with ground-based O_3 observations. In (~~a~~A), AIRS, MERRA2, and EAC4 O_3 data were spatially interpolated to the location of ozonesonde stations. In (~~b~~B), ground-based O_3 observations across 466 sites in 76 cities were resampled to EAC4 grid (0.75° × 0.75°) for comparison with EAC4-based surface ozone reanalysis; ground-based O_3 observations at three neighboring sites (Tiantan site in Beijing, Daishan Park site in Changchun, and Sham Shui Po site in Hong Kong) were used for comparison with Sonde-based surface ozone concentrations. *N*, *R*, MAB, RMSE, and IOA denote the number of statistic samples, correlation coefficient, mean absolute bias, root mean square error, and index of agreement, respectively.

~~**Table 1**. Evaluation statistics for commonly-used ozone products compared with the ozonesondes from Beijing, Changchun, and Hong Kong, and ground-based measurements across 76 cities in China~~

~~Variables~~	~~*R*~~	~~MAB (ppbv)~~	~~RMSE (ppbv)~~	~~IOA~~

~~O_3-AIRS & O_3-Sonde~~	~~0.793~~	~~67.2~~	~~122.1~~	~~0.907~~
~~O_3-MERRA2 & O_3-Sonde~~	~~0.939~~	~~27.3~~	~~43.5~~	~~0.981~~
~~O_3-EAC4 & O_3-Sonde~~	~~0.947~~	~~19.1~~	~~36.9~~	~~0.985~~
~~O_3-EAC4 & O_3-Ground~~	~~0.697~~	~~12.4~~	~~23.5~~	~~0.961~~

~~* *R*, MAB, RMSE, and IOA denote the correlation coefficient, mean absolute bias, root mean square error, and index of agreement, respectively.~~

Fig~~.~~. ~~3~~ 4 illustrates the EAC4-based three-dimensional structure of ~~high-level~~upper-level trough-induced stratospheric O_3~~ozone~~ intrusions over China. High O_3~~ozone~~ concentrations at 200 hPa aligned with the trough location, extending southwestward (June 10) and southward (June 11–13) along the trough axis, which well explained the ~~high-level~~upper-level secondary O_3~~ozone~~ peaks over Beijing since June 11 and over Changchun on June 13 (Fig. ~~2A~~ 2A and 2~~B~~B). The stratospheric intrusions developed into elongated (about 2000 km) and slender (about 200 km) streamers ~~At 400 hPa~~with elevated O_3 concentrations exceeding 150 ppbv (~~,~~referred to as ~~the~~ SDI-induced O_3-rich belts~~filament~~) at 400 hPa. On the east of the SDI streamers, the WCB streamers were parallel with anomalously low O_3 concentrations (referred to as WCB-related O_3-poor belts). ~~and WCB-related O_3-poor belt were distinguishable on each side of the trough axis, elongated approximately 2000 km and 200 km in width. This feature was most prominent on June 11, the day with the strongest stratospheric intrusion.~~ On June 12, the SDI-induced ~~SDI-induced~~ O_3-rich belt~~filament~~ ~~at 400 hPa~~ stretched to northeastern China, explaining the observed sub-high O_3~~ozone~~ ~~laminae~~ layer in the middle troposphere of Changchun (Fig. ~~2B~~2B). In the lower troposphere (700 hPa), ~~Considering no high-level secondary ozone peak in Changchun on this day, the middle-tropospheric high ozone laminae can be explained as a result of northward advection transport of the pre-intruded O_3-rich stratospheric air in the southern regions. Note that on June 11, the day with the strongest stratospheric intrusion, an~~ O_3-rich ~~filament~~ air masses appeared ~~in~~ over subtropical ~~the lower troposphere (700 hPa) of~~ southern China on June 11, the strongest SI day, indicating the southern edge of stratospheric O_3 intrusion. This lower-tropospheric O_3-rich ~~filament~~ air masses persisted in subsequent days and be exactly captured by Hong Kong's ozonesonde on June 13 (Fig. 2C). From June 11 to 13, there was a significant northeastward transport and dispersion of O_3-rich filament due to the strengthening southwesterly winds in the lower troposphere of eastern China. Through vertical and horizontal transport, lower tropospheric O_3~~ozone~~ concentrations increased by approximately 20 ppbv across eastern China, consistent with the 18 ppbv O_3~~ozone~~ increase observed in 2–6 km height over Beijing, indicating widespread enhancement of lower -tropospheric O_3~~ozone~~ background due to ~~ongoing~~ stratospheric O_3~~ozone~~ intrusion and accumulation.

Compared with total O_3~~ozone~~, ~~stratospheric ozone tracer (~~O_3S~~)~~ provides a more direct view of stratospheric intrusion (Fig. ~~3B~~4B). The three-dimensional O_3S structure depicts the ~~high-level~~upper-level trough-induced stratospheric O_3~~ozone~~ intrusion as a sheet-like lowering of the O_3S-rich layer along the western flank of the trough and an O_3S-rich tongue extending southward and westward from the trough base. These features aligned well with the typical structure of extratropical stratospheric intrusion associated with tropopause folding (Bithell et al., 1999;Hocking et al., 2007). On June 10, stratospheric O_3 intrusion directly hit the Tibetan Plateau, triggering extremely high surface O_3~~ozone~~ concentrations. From June 11 to 13, the O_3S-rich tongue progressed eastward into eastern China with the trough's eastward movement. Unlike that in the Tibetan Plateau, the O_3S-rich tongue in eastern China ~~penetrated to~~was blocked in the lower free troposphere ~~but was then blocked~~ and did not further intrude the surface layer. This result agreed well with the observed sub-high O_3~~ozone~~ ~~laminae~~ layer in 3.5–6.0 km height over Hong Kong (Fig. 2C), suggestive of no direct stratospheric O_3 intrusion to the surface in the low-elevation eastern China. Nevertheless, these O_3~~S~~-rich stratospheric air masses can be further transported into

~~the~~ atmospheric boundary layer via convective mixing pathway, contributing to boundary layer O_3~~ozone~~ increase. ~~However~~In this process, their stratospheric characteristics (high O_3~~ozone~~, low humidity) tend to be lost due to strong turbulence mixing, eventually becoming unrecognizable in ~~the~~ atmospheric boundary layer. Interestingly, another stratospheric intrusion induced by severe tropical storm (name: "Yagi") over the Northwest Pacific provided a parallel reference (Fig. ~~3B~~4B). Compared with the tropical storm-induced stratospheric O_3 instruction, the ~~high-level~~upper-level trough-induced ~~stratospheric~~ intrusion descended to a relatively lower altitude, causing widespread O_3S signals in the atmospheric boundary layer over eastern China. Note that apart from the trough- and storm-induced SI, a secondary SI emerged in the upwind of upper-level trough on June 12 likely driven by peripheral compensatory flows. This secondary SI lead to elevated O_3 concentrations over the Mongolian Plateau (Fig. 4A). However, they were not further transported into eastern China.

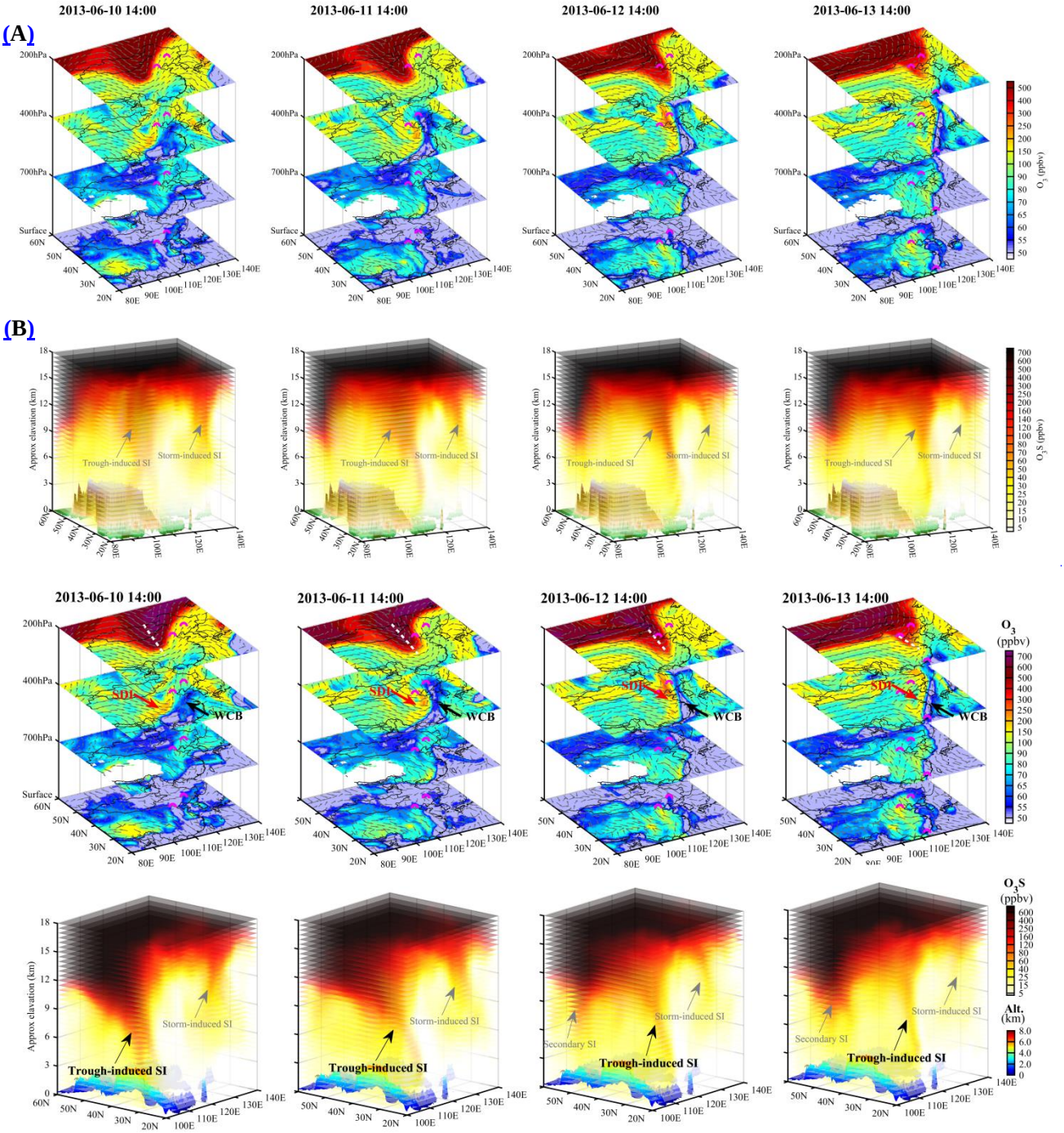

Fig. ~~3~~4. (A) Spatial distribution of ~~ozone~~ O_3 concentrations in 200, 400, 700 hPa, and surface layer. (B) Three-dimensional structure of ~~stratospheric ozone tracer~~ O_3S concentrations. In (A), white dashed lines mark the trough axis at 200 hPa, and m~~M~~agenta half-circles mark the locations of ozonesondes at different sites (Beijing, Changchun and Hong Kong) on different days.

3.3 Stratospheric intrusion contribution to surface O_3~~ozone~~ pollution

Fig. ~~4A~~ 5A presents the spatial distribution of surface O_3~~ozone~~ concentrations derived from ground-based measurements and EAC4 reanalysis during the SI event. The EAC4-based surface O_3~~ozone~~ reanalysis agreed well with nationwide ground-based observations (R = 0.697, MAB = 12.4 ppbv, RMSE = 23.5 ppbv, and IOA = 0.961, Fig. 3B), confirming the reliability of the EAC4 reanalysis again as the previous validation with ozonesondes. On June 10, the Tibetan Plateau experienced high O_3~~ozone~~ concentrations near or exceeding 80 ppbv, with observed O_3~~ozone~~ in Lhasa reaching up to 100 ppbv at 14:00 BJT. In contrast, eastern China exhibited low O_3~~ozone~~ concentrations (< 40 ppbv) due to cloudy and rainy weather on this day. From June 10 to 13, surface O_3~~ozone~~ concentrations decreased day by day in the Tibetan Plateau, while they increased from west to east in eastern China. By June 13, eastern China suffered severe O_3~~ozone~~ pollution, with observed O_3~~ozone~~ concentrations exceeding 100 ppbv in most of the NCP cities. From June 10 to 13, the continuous stratospheric dry intrusion led to a weather transition from cloudy to cloudless in eastern China (Fig. 1B), enhancing photochemical O_3~~ozone~~ production due to the abundance of O_3~~ozone~~ precursors over there. On the other hand, s~~S~~trong solar radiation in cloudless weather ~~also~~ promoted the development of thermal convection, facilitating the mixing of pre-intruded O_3-rich stratospheric air from the lower free troposphere into the surface layer. These two mechanisms combined to trigger severe O_3~~ozone~~ pollution in eastern China on June 13. The continue ozonesondes in Beijing provide convincing evidence for these two mechanisms. Returning to Fig. 2A, boundary-layer O_3~~ozone~~ concentrations in Beijing increased significantly from 57.8 ppbv on June 10 to 120.6 ppbv on June 13. Considering the sharp O_3~~ozone~~ gradient in the interface between the atmospheric boundary layer and the lower free troposphere, the dramatic increase in boundary-layer O_3~~ozone~~ can be primarily attributed to photochemical production (Liao et al., 2024). However, the concurrent rise in O_3~~ozone~~ concentrations in the lower free troposphere (an 18 ppbv O_3~~ozone~~ increase in 2–6 km height from June 10 to 13) indicated that stratospheric O_3~~ozone~~ intrusion contributed to elevating lower-tropospheric O_3~~ozone~~ background, ultimately exacerbating boundary layer O_3~~ozone~~ pollution.

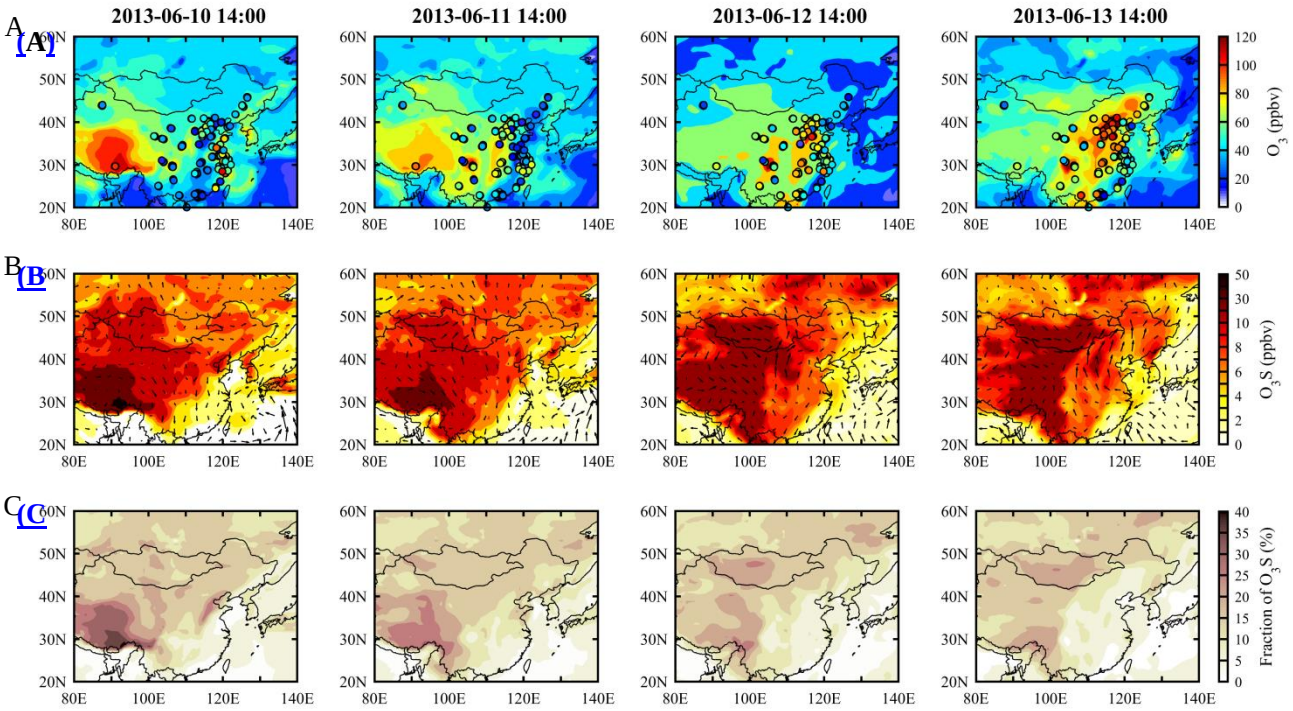

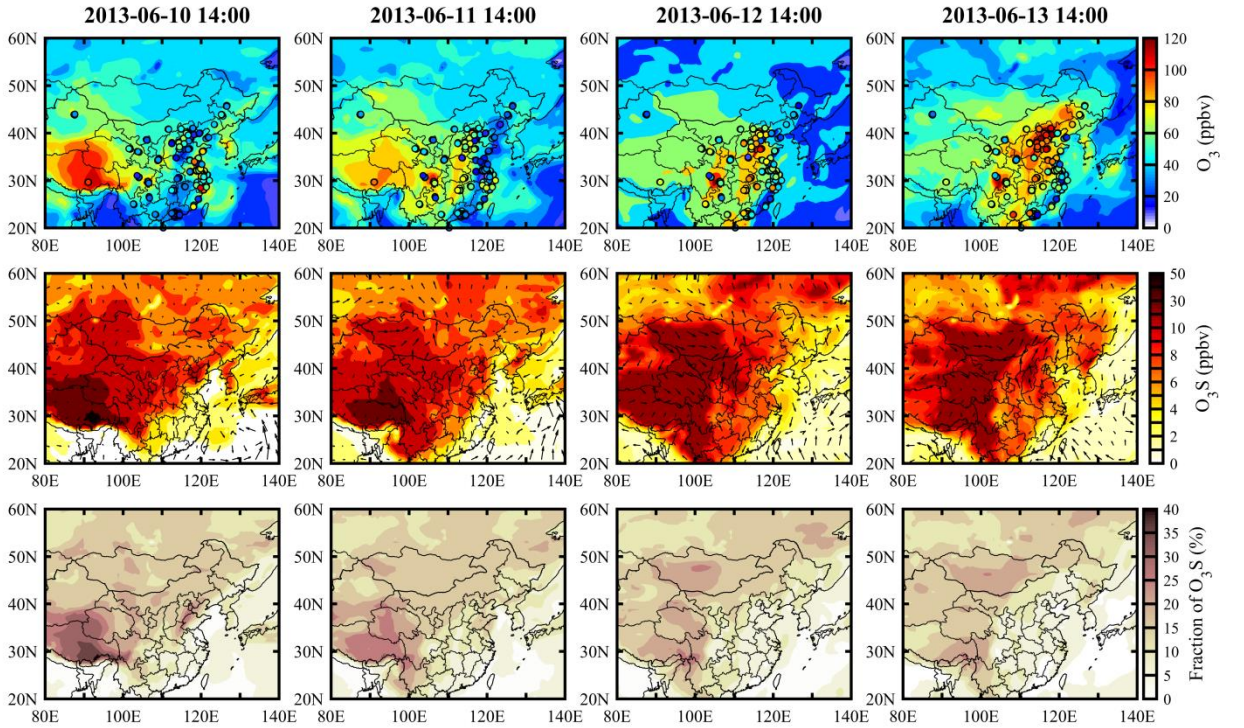

Fig. 45. (A) Surface spatial distribution of total ozone O_3 concentration derived from ground-based measurement (dots) and EAC4 reanalysis (shading). (B) Surface spatial distribution of stratospheric ozone tracerO_3S concentration derived from EAC4 reanalysis. (C) Surface spatial distribution of O_3Sstratospheric ozone tracer fraction in total surface O_3 concentration ozone calculated from EAC4 reanalysis.

To quantify the contribution of stratospheric ozone intrusion to surface O_3ozone pollution, Fig. 4B 5B illustrates the surface spatial distribution of EAC4-based surface stratospheric ozone tracer (O_3S) concentrations during the SI

event, and Fig. ~~4C~~ 5C shows the contribution fraction (CF) of O_3S in surface O_3 concentrations (CF = 100% × O_3S/O_3)~~ozone~~. The high-elevation Tibetan Plateau received high-concentration O_3~~ozone~~ from stratospheric intrusion, particularly on June 10 when the upper~~upper-~~level trough was oriented northeast-southwest towards the Tibetan Plateau. On this day, surface O_3S cocnentration exceeded 30 ppbv (up to 48.5 ppbv) in the Tibetan Plateau, contributing to over 30 % of the surface O_3~~ozone~~ concentration (up to 44.7 %). Subsequent days saw a gradual decrease in O_3S over the Tibetan Plateau~~ as it was dispersed eastward and then northward to the Mongolian Plateau~~. On June 12 and 13, significant O_3S hotspots (> 20 ppbv) appeared in the Mongolian Plateau. In conjunction with the ~~observed ozone profiles in Beijing (Fig. 2A) and the~~ three-dimensional O_3S structure (Fig. ~~3B~~4B), the elevated O_3S concentrations in the Mongolian Plateau ~~can be attributed~~can be attributed to the emerged ~~wind-driven dispersion of the intruded O_3-rich stratospheric air~~secondary SI on June 12 rather than ~~direct stratospheric intrusion at the local scale~~initial trough-induced SI. It seems that the elevated O_3S in the Mongolian Plateau had no influences on surface O_3 over eastern China considering its downwind location in the lower troposphere. Nonetheless, eastern China was affected not only by ~~Here, the intruded O_3-rich stratospheric air included the "aged" stratospheric air pre-intruded in the Tibetan Plateau and~~ the "fresh" stratospheric air in the eastward-movement O_3S-rich tongue (via convective mixing), but also by the pre-intruded "aged" stratospheric air from the Tibetan Plateau (via eastward transport)~~ over eastern China~~. Due to continuous ~~intrusion and~~ accumulation, ~~surface~~ region-averaged O_3S concentrations ~~also~~ increased approximately 1.0 ppbv in eastern China from June 10 to 13, whereas their fraction in surface O_3~~ozone~~ decreased from 11.8 % to 8.3 % as local O_3~~ozone~~ photochemical production accelerated~~ in the sunny weather~~. On June 13, surface O_3S concentrations in eastern China ranged from 3 to 15 ppbv, accounting for 2–10 % of surface O_3~~ozone~~ concentrations. I~~Two O_3S hotspots were identified in eastern China: one in the Taihang Mountains (10–15 ppbv) and another in southern NCP (8–10 ppbv). I~~n the highly polluted NCP region, ~~O_3S accounted for~~O_3S contributed approximately 10 % of surface O_3~~ozone concentrations~~, reflecting a nonnegligible role of stratospheric O_3 intrusion in exacerbating O_3 pollution~~significantly lower than the proportion in the Tibetan Plateau~~.

4 Conclusions and Discussion

This study reveals that the ~~high-level~~upper-level trough-induced stratospheric O_3~~ozone~~ intrusion over China did not occur as a local-scale vertical descent from the stratosphere to the lower troposphere just at the mid-latitude location where tropopause folding occurs; instead, it involved a long-range transport from mid-latitude tropopause folding zone (e.g., Beijing) to lower-latitude areas (e.g., Hong Kong), featuring an O_3-rich "tongue" structure with ~~high-level~~upper-level secondary O_3~~ozone~~ peak at the base of tongue (e.g., over Beijing) and lower-tropospheric sub-high O_3~~ozone~~ layer at the tip of tongue (e.g., over Hong Kong). The O_3-rich "tongue" swept through the high-elevation Tibetan Plateau when the ~~high-level~~upper-level trough extended towards this highland region at its initial stage, triggering extreme surface O_3~~ozone~~ pollution. With the eastward movement of ~~high-level~~upper-level trough, the O_3-rich "tongue" penetrated into the lower troposphere of low-elevation eastern China. Over there, the intruded O_3-rich stratospheric air masses in the lower troposphere, including ~~the "aged" stratospheric air horizontally transported from the Tibetan Plateau and~~ the "fresh" stratospheric air vertically transported from O_3-rich "tongue"~~,~~ and the "aged" stratospheric air horizontally transported from the Tibetan Plateau, were then entrained into the atmospheric boundary layer via lower-tropospheric dynamic processes (e.g. ~~subsidence motion and~~ convective mixing). At the same time, the strengthening lower-tropospheric southwesterly winds with the eastward movement of ~~high-level~~upper-level trough gradually participated to transport these O_3-rich stratospheric air back to the mid-latitudes, ultimately exacerbating surface O_3~~ozone~~ pollution in the NCP region (e.g., Beijing). While several SI events have been reported in China (Chang et al., 2023;Hong et al., 2024;Li et al., 2015;Luo et al., 2024;Wang et al., 2020a;Zhang et al., 2022;Zhao et al., 2024), this trough-induced SI episode may be the first event

of its widespread impact and refined structure documented (Fig. ~~5~~6).

The quantitative stratospheric intrusion contributions derived from the ~~fully-~~validated EAC4 reanalysis are generally consistent with previous model results in China. In the low-elevation eastern China, surface O_3S concentrations were previously estimated to be in the range of 5–20 ppbv during the SI events (Wang et al., 2020a;Zhang et al., 2022;Chang et al., 2023). Our EAC4-based estimation agreed well with this range, reflecting the typical magnitude of SI contribution in the low-elevation eastern China. As for the high-elevation Tibetan Plateau, a case-based model study (Skerlak et al., 2019) revealed that stratospheric tracer concentrations at the surface reach peak values of 20 % of the imposed stratospheric value, and a month-based model study (Yin et al., 2023) suggested that 36.5 % of surface O_3~~ozone~~ in the hotspot of the southern Tibetan Plateau was contributed by stratospheric O_3~~ozone~~ intrusion. Our EAC4-based estimation was comparable to these fractional contributions, corroborating the potential of SI to significantly influence surface O_3~~ozone~~ concentrations in this highland region. Besides, ground-based ~~stratospheric~~ chemical tracer method had been developed to quantify the stratospheric intrusion contribution over China. While Chen et al. (2024) identified the nationwide SI-induced O_3~~ozone~~ enhancement as a west-low-east-high spatial distribution pattern based on surface O_3~~ozone~~ and ~~carbon monoxide~~CO observations, Lin et al. (2021) determined a west-high-east-low spatial distribution pattern of SI-induced O_3~~ozone~~ contribution based on ground-based cosmogenic ^{35}S observations at the Himalayas and beyond. Our ~~fully-validated~~ result appears to support the latter, which conforms to the common knowledge that the highland regions are more susceptible to stratospheric intrusion because of their proximity to the stratosphere (Skerlak et al., 2019;Wang et al., 2020b;Lin et al., 2021).

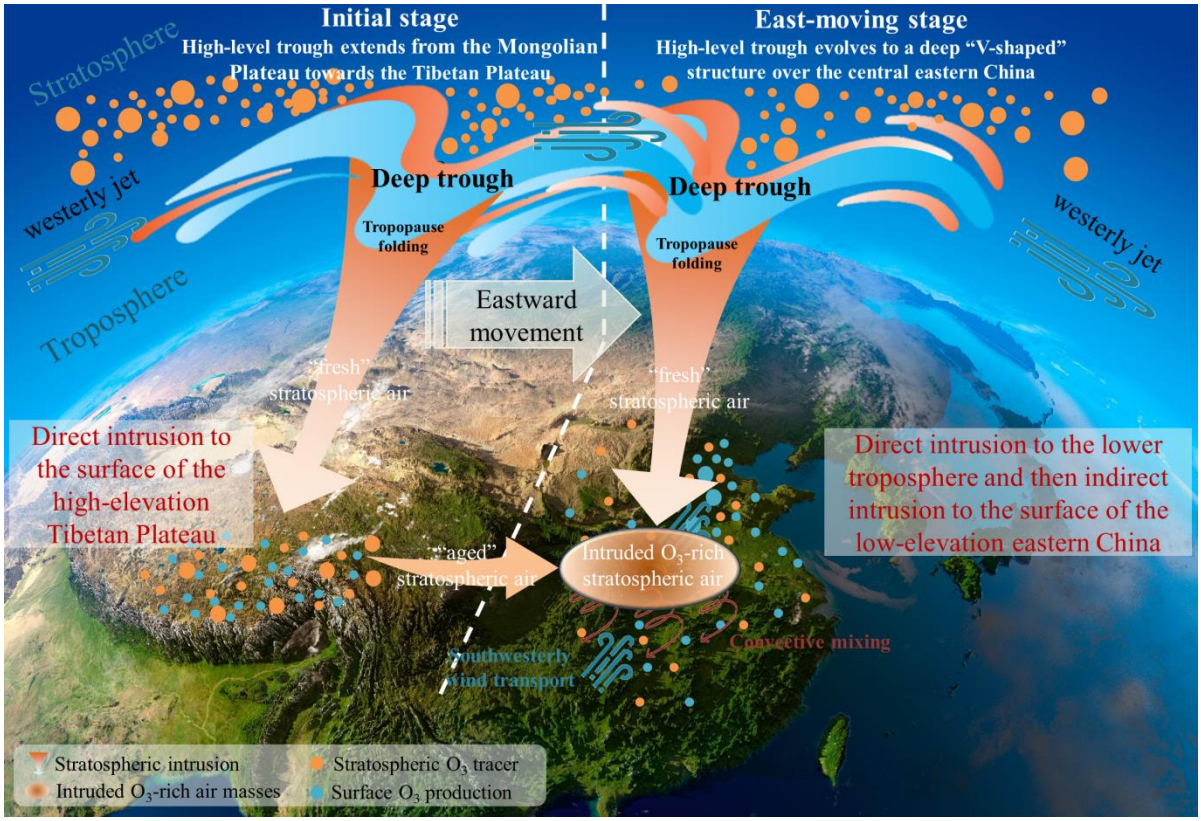

Fig. 5. Schematic illustration of ~~high-level~~upper-level trough-induced stratospheric ~~ozone~~ O_3 intrusion influence on surface ~~ozone~~ O_3 pollution over China

To the best of our knowledge, this study is the first to utilize continuous and multi-site ozonesondes to investigate

stratospheric O_3~~ozone~~ intrusion. While we acknowledge that a single case study may not be fully representative, it effectively demonstrates the value of continuous and multi-site ozonesonde measurements in enhancing our understanding of stratospheric O_3~~ozone~~ intrusion phenomena. On the other hand, these continuous and multi-site ozonesondes provide a valuable and unique benchmark for examining the capacity of those commonly-used O_3~~ozone~~ products (including AIRS satellite observation, MERRA2 and EAC4 O_3~~ozone~~ reanalysis) in characterizing stratospheric O_3~~ozone~~ intrusion. Previous study indicated that MERRA2 can be used in scientific studies to identify SIs by both atmospheric dynamics and composition (Knowland et al., 2017). Here, we demonstrate that EAC4, a publicly available dataset from European Centre for Medium-Range Weather Forecasts, performs better than MERRA2 in quantitatively characterizing stratospheric O_3~~ozone~~ intrusion via comparative evaluation. Moreover, in contrast to MERRA2, EAC4 simulates full O_3~~ozone~~ chemistry in the troposphere (an extended version of the Carbon Bond 2005 (CB05) chemical mechanism), allowing to determine the influence of stratospheric O_3~~ozone~~ on surface concentrations separate from photochemically produced O_3~~ozone~~. Therefore, this is a proof opening the door to detailed multiyear analyses of stratospheric O_3~~ozone~~ intrusion and their quantitative contribution to surface O_3~~ozone~~ over China and worldwide based on the publicly available EAC4 O_3~~ozone~~ reanalysis.

Data availability. All used data, excluding the ozonesonde in Beijing and Changchun, are open source. ERA5 atmospheric data are available from Copernicus Climate Change Service (C3S) Climate Data Store accessible at https://cds.climate.copernicus.eu/. EAC4 O_3~~ozone~~ reanalysis were obtained from Copernicus Atmospheric Monitoring Service Data Store accessible at https://ads.atmosphere.copernicus.eu/. The MODIS true color images are available from the NASA Earth Observations (NEO): https://neo.gsfc.nasa.gov/. The AIRS and MERRA2 O_3~~ozone~~ products were obtained from Goddard Earth Sciences Data and Information Services Center accessible at https://disc.gsfc.nasa.gov/. The ozonesonde data in Hong Kong were obtained from World Ozone and Ultraviolet Radiation Data Centre accessible at https://woudc.org/. The ozonesonde data in Beijing and Changchun are available from the first author upon reasonable request (zhliao@ium.cn).

Author contributions

Z.L. conceived the original idea, analyzed the data, and wrote the first version manuscript. J.Z. designed intensive ozonesonde experiments in Beijing and Changchun. Z.M supervised the research project. All authors discussed the results and commented on the manuscript.

Competing interests

The authors declare no competing interests.

Acknowledgements

This research has been supported by the National Natural Science Foundation of China (Grant Nos. 42405115, 42293321 and 42207115).

References

Akritidis, D., Katragkou, E., Zanis, P., Pytharoulis, I., Melas, D., Flemming, J., Inness, A., Clark, H., Plu, M., and Eskes, H.: A deep stratosphere-to-troposphere ozone transport event over Europe simulated in CAMS global and regional forecast systems: analysis and evaluation, Atmos Chem Phys, 18, 15515-15534, 10.5194/acp-18-15515-2018, 2018.

Appenzeller, C., and Davies, H. C.: Structure of stratospheric intrusions into the troposphere, Nature, 358, 570-572, 10.1038/358570a0, 1992.

Aumann, H. H., Chahine, M. T., Gautier, C., Goldberg, M. D., Kalnay, E., McMillin, L. M., Revercomb, H., Rosenkranz, P. W., Smith, W. L., Staelin, D. H., Strow, L. L., and Susskind, J.: AIRS/AMSU/HSB on the Aqua mission: design, science objectives, data products, and processing systems, IEEE Transactions on Geoscience and Remote Sensing, 41, 253-264, 10.1109/TGRS.2002.808356, 2003.

Bartusek, S., Wu, Y. T., Ting, M. F., Zheng, C., Fiore, A., Sprenger, M., and Flemming, J.: Higher-Resolution Tropopause Folding Accounts for More Stratospheric Ozone Intrusions, Geophys Res Lett, 50, ARTN e2022GL101690 10.1029/2022GL101690, 2023.

Bithell, M., Gray, L. J., and Cox, B. D.: A Three-Dimensional View of the Evolution of Midlatitude Stratospheric Intrusions, Journal of the Atmospheric Sciences, 56, 673-688, https://doi.org/10.1175/1520-0469(1999)056<0673:ATDVOT>2.0.CO;2, 1999.

Browning, K. A., and Roberts, N. M.: Structure of a frontal cyclone, Q J Roy Meteor Soc, 120, 1535-1557, https://doi.org/10.1002/qj.49712052006, 1994.

Browning, K. A.: The dry intrusion perspective of extra-tropical cyclone development, Meteorological Applications, 4, 317-324, https://doi.org/10.1017/S1350482797000613, 1997.

Chang, F. Y., Li, J. D., Li, N., and Liao, H.: Stratospheric intrusion may aggravate widespread ozone pollution through both vertical and horizontal advections in eastern China during summer, Front Env Sci-Switz, 10, Artn 1115746 10.3389/Fenvs.2022.1115746, 2023.

Chen, X. L., Ma, Y. M., Kelder, H., Su, Z., and Yang, K.: On the behaviour of the tropopause folding events over the Tibetan Plateau, Atmos Chem Phys, 11, 5113-5122, 10.5194/acp-11-5113-2011, 2011.

Chen, Z., Liu, J., Qie, X., Cheng, X., Yang, M., Shu, L., and Zang, Z.: Stratospheric influence on surface ozone pollution in China, Nat Commun, 15, 4064, 10.1038/s41467-024-48406-x, 2024.

Chen, Z. X., Liu, J. E., Cheng, X. G., Yang, M. M., and Shu, L.: Stratospheric influences on surface ozone increase during the COVID-19 lockdown over northern China, Npj Clim Atmos Sci, 6, Artn 76 10.1038/S41612-023-00406-2, 2023.

Cristofanelli, P., Bracci, A., Sprenger, M., Marinoni, A., Bonafè, U., Calzolari, F., Duchi, R., Laj, P., Pichon, J. M., Roccato, F., Venzac, H., Vuillermoz, E., and Bonasoni, P.: Tropospheric ozone variations at the Nepal Climate Observatory-Pyramid (Himalayas, 5079 m a.s.l.) and influence of deep stratospheric intrusion events, Atmos Chem Phys, 10, 6537-6549, 10.5194/acp-10-6537-2010, 2010.

Dreessen, J.: A Sea Level Stratospheric Ozone Intrusion Event Induced within a Thunderstorm Gust Front, B Am Meteorol Soc, 100, 1259-1275, 10.1175/Bams-D-18-0113.1, 2019.

Gelaro, R., McCarty, W., Suárez, M. J., Todling, R., Molod, A., Takacs, L., Randles, C. A., Darmenov, A., Bosilovich, M. G., Reichle, R., Wargan, K., Coy, L., Cullather, R., Draper, C., Akella, S., Buchard, V., Conaty, A., da Silva, A. M., Gu, W., Kim, G.-K., Koster, R., Lucchesi, R., Merkova, D., Nielsen, J. E., Partyka, G., Pawson, S., Putman, W., Rienecker, M., Schubert, S. D., Sienkiewicz, M., and Zhao, B.: The Modern-Era Retrospective Analysis for Research and Applications, Version 2 (MERRA-2), Journal of Climate, 30, 5419-5454, https://doi.org/10.1175/JCLI-D-16-0758.1, 2017.

Granier, C., Bessagnet, B., Bond, T., D'Angiola, A., Denier van der Gon, H., Frost, G. J., Heil, A., Kaiser, J. W., Kinne, S., Klimont, Z., Kloster, S., Lamarque, J.-F., Liousse, C., Masui, T., Meleux, F., Mieville, A., Ohara, T., Raut, J.-C., Riahi, K., Schultz, M. G., Smith, S. J., Thompson, A., van Aardenne, J., van der Werf, G. R., and van Vuuren, D. P.: Evolution of anthropogenic and biomass burning emissions of air pollutants at global and regional scales during the 1980–2010 period, Climatic Change, 109, 163, 10.1007/s10584-011-0154-1, 2011.

Guenther, A., Karl, T., Harley, P., Wiedinmyer, C., Palmer, P. I., and Geron, C.: Estimates of global terrestrial isoprene emissions using MEGAN (Model of Emissions of Gases and Aerosols from Nature), Atmos. Chem. Phys., 6, 3181-3210, 10.5194/acp-6-3181-2006, 2006.

Hersbach, H., Bell, B., Berrisford, P., Hirahara, S., Horányi, A., Muñoz-Sabater, J., Nicolas, J., Peubey, C., Radu, R.,

Schepers, D., Simmons, A., Soci, C., Abdalla, S., Abellan, X., Balsamo, G., Bechtold, P., Biavati, G., Bidlot, J., Bonavita, M., De Chiara, G., Dahlgren, P., Dee, D., Diamantakis, M., Dragani, R., Flemming, J., Forbes, R., Fuentes, M., Geer, A., Haimberger, L., Healy, S., Hogan, R. J., Hólm, E., Janisková, M., Keeley, S., Laloyaux, P., Lopez, P., Lupu, C., Radnoti, G., de Rosnay, P., Rozum, I., Vamborg, F., Villaume, S., and Thépaut, J. N.: The ERA5 global reanalysis, Q J Roy Meteor Soc, 146, 1999-2049, 10.1002/qj.3803, 2020.

Hocking, W. K., Carey-Smith, T., Tarasick, D. W., Argall, P. S., Strong, K., Rochon, Y., Zawadzki, I., and Taylor, P. A.: Detection of stratospheric ozone intrusions by windprofiler radars, Nature, 450, 281-284, 10.1038/nature06312, 2007.

Hong, J., Wang, H., Wang, W., Zhu, J., Deng, H., and Wang, H.: Impacts of stratosphere-to-troposphere transport on tropospheric ozone in southeastern China: insights from ozonesonde observations, Environ Res Lett, 19, 064068, 10.1088/1748-9326/ad4ef9, 2024.

Hwang, S. H., Kim, J., and Cho, G. R.: Observation of secondary ozone peaks near the tropopause over the Korean peninsula associated with stratosphere-troposphere exchange, J Geophys Res-Atmos, 112, Artn D16305 10.1029/2006jd007978, 2007.

Inness, A., Ades, M., Agusti-Panareda, A., Barré, J., Benedictow, A., Blechschmidt, A. M., Dominguez, J. J., Engelen, R., Eskes, H., Flemming, J., Huijnen, V., Jones, L., Kipling, Z., Massart, S., Parrington, M., Pench, V. H., Razinger, M., Remy, S., Schulz, M., and Suttie, M.: The CAMS reanalysis of atmospheric composition, Atmos Chem Phys, 19, 3515-3556, 10.5194/acp-19-3515-2019, 2019.

Jaeglé, L., Wood, R., and Wargan, K.: Multiyear Composite View of Ozone Enhancements and Stratosphere-to-Troposphere Transport in Dry Intrusions of Northern Hemisphere Extratropical Cyclones, Journal of Geophysical Research: Atmospheres, 122, 13,436-413,457, https://doi.org/10.1002/2017JD027656, 2017.

Jordan, C. E., Dibb, J. E., and Finkel, R. C.: 10Be/7Be tracer of atmospheric transport and stratosphere-troposphere exchange, Journal of Geophysical Research: Atmospheres, 108, https://doi.org/10.1029/2002JD002395, 2003.

Kaiser, J. W., Heil, A., Andreae, M. O., Benedetti, A., Chubarova, N., Jones, L., Morcrette, J. J., Razinger, M., Schultz, M. G., Suttie, M., and van der Werf, G. R.: Biomass burning emissions estimated with a global fire assimilation system based on observed fire radiative power, Biogeosciences, 9, 527-554, 10.5194/bg-9-527-2012, 2012.

Knowland, K. E., Ott, L. E., Duncan, B. N., and Wargan, K.: Stratospheric Intrusion-Influenced Ozone Air Quality Exceedances Investigated in the NASA MERRA-2 Reanalysis, Geophys Res Lett, 44, 10691-10701, 10.1002/2017GL074532, 2017.

Langford, A. O., Brioude, J., Cooper, O. R., Senff, C. J., Alvarez, R. J., Hardesty, R. M., Johnson, B. J., and Oltmans, S. J.: Stratospheric influence on surface ozone in the Los Angeles area during late spring and early summer of 2010, J Geophys Res-Atmos, 117, Artn D00v06 10.1029/2011jd016766, 2012.

Lemoine, R.: Secondary maxima in ozone profiles, Atmos Chem Phys, 4, 1085-1096, DOI 10.5194/acp-4-1085-2004, 2004.

Li, D., Bian, J. C., and Fan, Q. J.: A deep stratospheric intrusion associated with an intense cut-off low event over East Asia, Sci China Earth Sci, 58, 116-128, 10.1007/s11430-014-4977-2, 2015.

Liao, Z., Gao, M., Zhang, J., Sun, J., Quan, J., Jia, X., Pan, Y., and Fan, S.: Mixing-layer-height-referenced ozone vertical distribution in the lower troposphere of Chinese megacities: stratification, classification, and meteorological and photochemical mechanisms, Atmos. Chem. Phys., 24, 3541-3557, 10.5194/acp-24-3541-2024, 2024.

Lin, M., Su, L., Shaheen, R., Fung, J. C. H., and Thiemens, M. H.: Detection of deep stratospheric intrusions by cosmogenic ^{35}S, P Natl Acad Sci USA, 113, 11131-11136, 10.1073/pnas.1609919113, 2016.

Lin, M., Wang, K., Kang, S., Li, Y., Fan, Z., and Thiemens, M. H.: Isotopic signatures of stratospheric air at the Himalayas and beyond, Sci Bull, 66, 323-326, https://doi.org/10.1016/j.scib.2020.11.005, 2021.

Lin, M. Y., Fiore, A. M., Horowitz, L. W., Langford, A. O., Oltmans, S. J., Tarasick, D., and Rieder, H. E.: Climate variability

modulates western US ozone air quality in spring via deep stratospheric intrusions, Nat Commun, 6, Artn 7105 10.1038/Ncomms8105, 2015.

Liu, X., Fu, Y., Zhang, L., Li, H., Burr, G. S., Bi, Y., and Zhao, G.: Deep stratospheric intrusion events in China revealed on the ground by cosmogenic 10Be/7Be, Communications Earth & Environment, 5, 553, 10.1038/s43247-024-01727-7, 2024.

Luo, Y., Zhao, T., Meng, K., Hu, J., Yang, Q., Bai, Y., Yang, K., Fu, W., Tan, C., Zhang, Y., Zhang, Y., and Li, Z.: A mechanism of stratospheric O3 intrusion into the atmospheric environment: a case study of the North China Plain, Atmos. Chem. Phys., 24, 7013-7026, 10.5194/acp-24-7013-2024, 2024.

Ma, J., Lin, W. L., Zheng, X. D., Xu, X. B., Li, Z., and Yang, L. L.: Influence of air mass downward transport on the variability of surface ozone at Xianggelila Regional Atmosphere Background Station, southwest China, Atmos Chem Phys, 14, 5311-5325, 10.5194/acp-14-5311-2014, 2014.

Monks, P. S., Archibald, A. T., Colette, A., Cooper, O., Coyle, M., Derwent, R., Fowler, D., Granier, C., Law, K. S., Mills, G. E., Stevenson, D. S., Tarasova, O., Thouret, V., von Schneidemesser, E., Sommariva, R., Wild, O., and Williams, M. L.: Tropospheric ozone and its precursors from the urban to the global scale from air quality to short-lived climate forcer, Atmos Chem Phys, 15, 8889-8973, 10.5194/acp-15-8889-2015, 2015.

Ojha, N., Pozzer, A., Akritidis, D., and Lelieveld, J.: Secondary ozone peaks in the troposphere over the Himalayas, Atmos Chem Phys, 17, 6743-6757, 10.5194/acp-17-6743-2017, 2017.

Ou-Yang, C. F., Babu, S. R., Lee, J. R., Yen, M. C., Griffith, S. M., Lin, C. C., Chang, S. C., and Lin, N. H.: Detection of stratospheric intrusion events and their role in ozone enhancement at a mountain background site in sub-tropical East Asia, Atmos Environ, 268, ARTN 118779 10.1016/j.atmosenv.2021.118779, 2022.

Skerlak, B., Pfahl, S., Sprenger, M., and Wernli, H.: A numerical process study on the rapid transport of stratospheric air down to the surface over western North America and the Tibetan Plateau, Atmos Chem Phys, 19, 6535-6549, 10.5194/acp-19-6535-2019, 2019.

Stohl, A., Bonasoni, P., Cristofanelli, P., Collins, W., Feichter, J., Frank, A., Forster, C., Gerasopoulos, E., Gäggeler, H., James, P., Kentarchos, T., Kromp-Kolb, H., Krüger, B., Land, C., Meloen, J., Papayannis, A., Priller, A., Seibert, P., Sprenger, M., Roelofs, G. J., Scheel, H. E., Schnabel, C., Siegmund, P., Tobler, L., Trickl, T., Wernli, H., Wirth, V., Zanis, P., and Zerefos, C.: Stratosphere-troposphere exchange: A review, and what we have learned from STACCATO, J Geophys Res-Atmos, 108, Artn 8516 10.1029/2002jd002490, 2003.

Wang, H. Y., Wang, W., Huang, X., and Ding, A. J.: Impacts of stratosphere-to-troposphere-transport on summertime surface ozone over eastern China, Sci Bull, 65, 276-279, 10.1016/j.scib.2019.11.017, 2020a.

Wang, X. Y., Wu, Y. T., Randel, W., and Tilmes, S.: Stratospheric contribution to the summertime high surface ozone events over the western united states, Environ Res Lett, 15, ARTN 1040a6 10.1088/1748-9326/abba53, 2020b.

Yates, E. L., Iraci, L. T., Roby, M. C., Pierce, R. B., Johnson, M. S., Reddy, P. J., Tadic, J. M., Loewenstein, M., and Gore, W.: Airborne observations and modeling of springtime stratosphere-to-troposphere transport over California, Atmos Chem Phys, 13, 12481-12494, 10.5194/acp-13-12481-2013, 2013.

Yin, X. F., Rupakheti, D., Zhang, G. S., Luo, J. L., Kang, S. C., de Foy, B., Yang, J. H., Ji, Z. M., Cong, Z. Y., Rupakheti, M., Li, P., Hu, Y. L., and Zhang, Q. G.: Surface ozone over the Tibetan Plateau controlled by stratospheric intrusion, Atmos Chem Phys, 23, 10137-10143, 10.5194/acp-23-10137-2023, 2023.

Zhang, J.-q., Xuan, Y., Xia, X.-A., Liu, M., Yan, X.-l., Pang, L., Bai, Z.-X., and Wang, X.: Performance Evaluation of a Self-Developed Ozonesonde and Its Application in an Intensive Observational Campaign, Atmospheric and Oceanic Science Letters, 7, 175 - 179, 2013.

Zhang, J., Gong, X., Crosbie, E., Diskin, G., Froyd, K., Hall, S., Kupc, A., Moore, R., Peischl, J., Rollins, A., Schwarz, J., Shook, M., Thompson, C., Ullmann, K., Williamson, C., Wisthaler, A., Xu, L., Ziemba, L., Brock, C. A., and Wang, J.: Stratospheric air intrusions promote global-scale new particle formation, Science, 385, 210-216, 10.1126/science.adn2961, 2024.

Zhang, J. Q., Li, D., Bian, J. C., Xuan, Y. J., Chen, H. B., Bai, Z. X., Wan, X. W., Zheng, X. D., Xia, X. G., and Lu, D. R.: Long-term ozone variability in the vertical structure and integrated column over the North China Plain: results based on ozonesonde and Dobson measurements during 2001-2019, Environ Res Lett, 16, Artn 074053 10.1088/1748-9326/Ac109f, 2021.

Zhang, Y. J., Li, J., Yang, W. Y., Du, H. Y., Tang, X., Ye, Q., Wang, Z. X., Sun, Y. L., Pan, X. L., Zhu, L. L., and Wang, Z. F.: Influences of stratospheric intrusions to high summer surface ozone over a heavily industrialized region in northern China, Environ Res Lett, 17, Artn 094023 10.1088/1748-9326/Ac8b24, 2022.

Zhao, K., Chen, Y., Lian, P., Li, W., Yang, F., Zhang, X., and Yang, R.: Impact of stratospheric intrusions on surface ozone enhancement in Hong Kong in the lower troposphere: Implications for ozone control strategy, Atmos Environ, 329, 120539, https://doi.org/10.1016/j.atmosenv.2024.120539, 2024.

Zhao, K., Chen, W., Lian, P., and Xu, D.: Optimizing Ozone Control Strategies for Chinese Megacity Clusters Under the Influence of Stratospheric Intrusion, Journal of Geophysical Research: Atmospheres, 130, e2024JD043112, https://doi.org/10.1029/2024JD043112, 2025.

Zhao, K. H., Huang, J. P., Wu, Y. H., Yuan, Z. B., Wang, Y. W., Li, Y., Ma, X. D., Liu, X. H., Ma, W., Wang, Y., and Zhang, X. Y.: Impact of Stratospheric Intrusions on Ozone Enhancement in the Lower Troposphere and Implication to Air Quality in Hong Kong and Other South China Regions, J Geophys Res-Atmos, 126, ARTN e2020JD033955 10.1029/2020JD033955, 2021.

Zheng, X., Yang, W., Sun, Y., Geng, C., Liu, Y., and Xu, X.: Comment on “Transport of substantial stratospheric ozone to the surface by a dying typhoon and shallow convection” by Chen et al. (2022), Atmos. Chem. Phys., 24, 3759-3768, 10.5194/acp-24-3759-2024, 2024.

Zhu, F., Luo, J., Wang, Z., Jin, H., Zhao, Q., Wang, Z., Luo, F., and Gu, M.: The Impact of Stratosphere-to-Troposphere Transport Associated with the Northeast China Cold Vortex on Surface Ozone Concentrations in Eastern China, Journal of Applied Meteorology and Climatology, https://doi.org/10.1175/JAMC-D-24-0027.1, 2024.